

Structure and scaling of Kitaev chain across a quantum critical point in real space

Yan He¹ and Chih-Chun Chien²

¹*College of Physics, Sichuan University, Chengdu, Sichuan 610064, China**

²*Department of Physics, University of California, Merced, CA 95343, USA.†*

The spatial Kibble-Zurek mechanism (KZM) is applied to the Kitaev chain with inhomogeneous pairing interactions that vanish in half of the lattice and result in a quantum critical point separating the superfluid and normal-gas phases in real space. The weakly-interacting BCS theory predicts scaling behavior of the penetration of the pair wavefunction into the normal-gas region different from conventional power-law results due to the non-analytic dependence of the BCS order parameter on the interaction. The Bogoliubov-de Gennes (BdG) equation produces numerical results confirming the scaling behavior and hints complications in the strong-interaction regime. The limiting case of the step-function quench shows the dominance of the BCS coherence length in absence of additional length scale. Furthermore, the energy spectrum and wavefunctions from the BdG equation show abundant in-gap states from the normal-gas region in addition to the topological edge states.

I. INTRODUCTION

A quantum phase transition (QPT) occurs when a change of the Hamiltonian leads to different phases of matter in the ground state, see Refs. [1–5] for a review. The transverse-field Ising model (TFIM) serves as an exactly solvable model for a clear demonstration of a QPT as the magnetic field crosses a critical value and changes the magnetic order. On the other hand, the BCS theory of fermionic superfluid provides a mean-field description of off-diagonal long-range order induced by attractive interactions [6]. Shutting off the pairing interaction at zero temperature turns the superfluid into a normal Fermi gas through a QPT. Similar to conventional phase transitions, universal scaling behavior emerges near a QPT with diverging correlation length and time.

While conventional ways of studying QPTs focus on homogeneous systems in the thermodynamic limit, here we will take a different route and investigate a QPT in real space induced by an inhomogeneous form of the Hamiltonian, where a spatially changing parameter results in a symmetric phase and a symmetry-broken phase separated by a quantum critical point (QCP) in real space. Explicitly, we will follow the framework of the spatial Kibble-Zurek mechanism (KZM) [7–11] to analyze the remnant of the order parameter from the symmetry-broken phase into the symmetric phase when the whole system is in equilibrium. Previous studies of the spatial KZM on the inhomogeneous TFIM [7, 8] and atomic spinor gases [9] have revealed interesting scaling behavior with exponents reflecting the critical exponents of the corresponding homogeneous systems. On the other hand, Ref. [12] shows that the non-analytic expression of the order parameter of the BCS theory of a Fermi superfluid with s -wave pairing leads to more complex scaling behavior when a QPT in real space is induced by inhomogeneous pairing interactions.

Here we apply the spatial KZM to a p -wave Fermi superfluid, which in 1D has the form of the Kitaev chain [13]. The inhomogeneous pairing interaction drops to zero in real space to generate a QCP separating the superfluid and normal Fermi gas on the two sides. A linear ramp of the interaction introduces a frozen length scale [10] through the slope of the ramp that combines with the BCS theory to produce interesting scaling behavior on the normal-gas side. Another type of quenches of the interaction profiles, called the step-function quench, has a sudden drop of the parameter across the critical point in real space and may be viewed as a limiting case of the spatial quench as the ramping rate goes to infinity. A previous study [12] of the step-function quench of s -wave BCS superfluids in continuum reveals that the BCS coherence length becomes the only relevant length scale in the weak-interaction regime.

We will set up the Bogoliubov-de Gennes (BdG) equation [14, 15] of the Kitaev chain of a p -wave Fermi superfluid with inhomogeneous interaction profiles to analyze the structure, scaling behavior, and spectrum as the system exhibits a QCP in real space due to the vanishing of the interactions in part of the lattice. The Kitaev chain is a paradigm of topological superconductors [16–18] and may host Majorana bound states [13, 19]. The BdG formalism allows us to analyze the energy spectrum of the Kitaev chain across a QCP in real space. We will show that, in addition to the topological edge states near zero energy due to the hard-wall confinement, the normal-gas region introduce abundant in-gap states localized on the region with zero pairing interaction.

Before presenting our studies, we remark on the difference between the time-independent KZM studied here and the time-dependent KZM, which was the original idea of analyzing structures across phase transitions [20–22] and is more common in the literature [10, 23–26]. For the time-dependent KZM, the system is homogeneous but driven out of equilibrium by a linear ramp of a parameter in time of the form t/τ_Q . The scaling is determined by the quench rate $1/\tau_Q$, and topological defects may emerge in such nonequilibrium settings [27–30]. In contrast, the spatial KZM keeps the system in equilib-

* heyan_ctp@scu.edu.cn

† cchien5@ucmerced.edu

rium but introduces a linear ramp of a parameter in real space of the form $\alpha(x - x_c)$, where x_c is the location of the transition and α is the quench rate in space. To establish equilibrium between the two sides of the critical point in real space produced by the spatially varying parameter, scaling behavior depending on α will emerge in the time-independent KZM and reveal properties of the corresponding homogeneous systems. More contrasts between time-dependent and time-independent KZMs can be found in Refs. [10, 12]. While there have been many theoretical [31–39] and experimental [40–51] studies on the time-dependent KZM, the time-independent KZM has been less explored and awaits more investigations.

The rest of the paper is organized as follows. Sec. II briefly summarizes the Kitaev chain in the homogeneous case and the BdG formalism for solving an inhomogeneous Kitaev chain. Sec. III introduces the spatial and step-function quenches and reviews their scaling mechanisms. Sec. IV presents the profiles, scaling analyses, energy spectrum, and eigenfunctions of the Kitaev chain with inhomogeneous pairing interactions. The agreements with the weak-interaction predictions and deviations when the interaction is strong are demonstrated. We also discuss physical implications and relevance to previous works. Finally, Sec. V concludes our work.

II. THEORETICAL BACKGROUND OF KITAEV CHAIN

A. Homogeneous systems

The Kitaev chain is a model of a spinless Fermi superfluid with p -wave pairing. The Hamiltonian in real space is given by

$$H = \sum_i \left[-w(c_i^\dagger c_{i+1} + c_{i+1}^\dagger c_i) - \mu c_i^\dagger c_i + \Delta(c_i^\dagger c_{i+1}^\dagger + c_{i+1} c_i) \right]. \quad (1)$$

Here c_i and c_i^\dagger are the fermion annihilation and creation operators on site i , w is the hopping coefficient, and Δ is the gap function of the nearest-neighbor pairing. We set $\hbar = 1 = k_B$ throughout the paper and use w and the lattice constant a as the energy and length units, respectively.

For a homogeneous system with periodic boundary condition, the Hamiltonian in momentum space in terms of the Nambu spinor $\psi = (c_k, c_{-k}^\dagger)^T$ is given by

$$H = \begin{pmatrix} -2w \cos k - \mu & -2i\Delta \sin k \\ 2i\Delta \sin k & 2w \cos k + \mu \end{pmatrix} = d_3 \sigma_3 + d_2 \sigma_2. \quad (2)$$

Here $d_3 = -2w \cos k - \mu$, $d_2 = 2\Delta \sin k$, and σ_i with $i = 1, 2, 3$ are the Pauli matrices applying to the Nambu

space. The Hamiltonian satisfy the particle-hole symmetry

$$\sigma_1 H^*(-k) \sigma_1 = -H(k). \quad (3)$$

Therefore, this model belongs to the class D, which has a \mathbb{Z}_2 index in 1D [18]. The eigenvalues of the above Hamiltonian are given by

$$E = \pm E_k, \quad E_k = \sqrt{d_2^2 + d_3^2}, \quad (4)$$

The eigenstate of the lower band can be written as

$$|\psi\rangle = \left(v_k, i \operatorname{sgn}(d_2) u_k \right)^T. \quad (5)$$

Here $u_k = \sqrt{\frac{E_k + d_3}{2E_k}}$ and $v_k = \sqrt{\frac{E_k - d_3}{2E_k}}$.

The gap function is defined as $\Delta = g \langle c_i c_{i+1} \rangle$, where g is the coupling constant of the attraction between fermions. Following the BCS theory, the gap equation for a system of size L at $T = 0$ is given by

$$\frac{1}{g} = \frac{1}{L} \sum_k \frac{2 \sin^2 k}{E_k}. \quad (6)$$

For the half-filling case, $\mu = 0$ and we find that

$$\begin{aligned} \frac{1}{L} \sum_k \frac{2 \sin^2 k}{E_k} &= \frac{1}{2\pi} \int_0^{2\pi} \frac{\sin^2 k dk}{\sqrt{w^2 \cos^2 k + \Delta^2 \sin^2 k}} \\ &= \frac{2}{\pi w (1 - \Delta^2/w^2)} \left[K \left(\sqrt{1 - \frac{\Delta^2}{w^2}} \right) - E \left(\sqrt{1 - \frac{\Delta^2}{w^2}} \right) \right] \end{aligned} \quad (7)$$

Here we have used the complete elliptic integral

$$\begin{aligned} K(q) &= \int_0^{\pi/2} \frac{dx}{\sqrt{1 - q^2 \sin^2 x}}, \\ E(q) &= \int_0^{\pi/2} \sqrt{1 - q^2 \sin^2 x} dx. \end{aligned} \quad (8)$$

For $q' = \sqrt{1 - q^2} \ll 1$, $K(q)$ can be approximated as

$$K(q) = \ln \frac{4}{q'} + O((q')^2), \quad E(q) = 1 + O((q')^2). \quad (9)$$

Since $\Delta \ll w$ in the weakly-interacting regime, the gap equation becomes

$$\frac{1}{g} \approx \frac{2}{\pi w} \left(\ln \frac{4w}{\Delta} - 1 \right). \quad (10)$$

The gap function at $T = 0$ in the weakly-interacting regime thus has the expression

$$\Delta \approx 4w \exp\left(-\frac{\pi w}{2g} - 1\right). \quad (11)$$

Since Δ is non-analytic in g , interesting scaling behavior will emerge in our study of inhomogeneous systems.

The BCS coherence length at $T = 0$ is roughly the size of a Cooper pair [6], which is given by

$$\xi_0^2 = \frac{\langle \psi_k | -\nabla_k^2 | \psi_k \rangle}{\langle \psi_k | \psi_k \rangle}. \quad (12)$$

Here $\psi_k = u_k v_k = \frac{\Delta \sin k}{2E_k}$ is the Cooper pair wavefunction, and u_k, v_k are given below Eq. (5). For the superfluid with p -wave pairing, we have

$$\langle \psi_k | -\nabla_k^2 | \psi_k \rangle = \sum_k \left(\frac{d\psi_k}{dk} \right)^2 = \frac{\pi(w^2 + 3\Delta^2)}{16w\Delta}, \quad (13)$$

$$\langle \psi_k | \psi_k \rangle = \sum_k \psi_k^2 = \frac{\pi\Delta}{2(\Delta + w)}. \quad (14)$$

Thus,

$$\xi_0 \approx \frac{w}{2\sqrt{2}\Delta}. \quad (15)$$

Combining with Eq. (11), one obtains the following scaling behavior of the BCS coherence length:

$$\ln(\xi_0) \sim g^{-1}. \quad (16)$$

The topology of the Kitaev chain is characterized by the Berry phase in 1D, which is computed as

$$\begin{aligned} \theta &= i \int_0^{2\pi} dk \langle \psi | \frac{\partial}{\partial k} | \psi \rangle \\ &= \frac{i}{2} \int_0^{2\pi} dk \frac{\partial}{\partial k} \ln[\text{sgn}(d_2)] \left(1 + \frac{d_3}{E_k} \right). \end{aligned} \quad (17)$$

One can show that

$$\theta = \begin{cases} \pi, & 2w > \mu, \\ 0, & 2w < \mu. \end{cases} \quad (18)$$

The bulk-boundary correspondence of topological systems [16–18] relates the topological index in the bulk with the localized edge states at the boundary. Localized edge states with zero eigen-energy appear in the Kitaev chain with open boundary condition when the Berry phase of the corresponding system with periodic boundary condition takes the nontrivial value $\theta = \pi$. When $\theta = 0$ in a periodic Kitaev chain, the system is topologically trivial and there is no localized edge state in the corresponding open chain.

B. BdG equation for inhomogeneous cases

Here we consider a Kitaev chain with a spatially dependent coupling constant g_i , as illustrated in Fig. 1. The Hamiltonian is similar to Eq. (1) with a spatially dependent gap function

$$\Delta_i = g_i \langle c_i c_{i+1} \rangle. \quad (19)$$

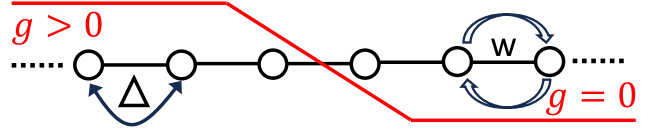


Figure 1. Illustration of the Kitaev chain with inhomogeneous pairing interactions (red solid line). A linear ramp (sudden drop) corresponds to a spatial (step-function) quench. The nearest-neighbor pairing gap Δ and hopping coefficient w are also shown.

Explicitly,

$$H = \sum_{i,j} \left[T_{ij} c_i^\dagger c_j + \frac{1}{2} V_{ij} c_i^\dagger c_j^\dagger + \frac{1}{2} V_{ij} c_j c_i \right], \quad (20)$$

where $T_{ij} = -w(\delta_{i+1,j} + \delta_{i,j+1}) - \mu\delta_{ij}$ and $V_{ij} = \Delta_i(\delta_{i+1,j} - \delta_{i,j+1})$. The Hamiltonian can be diagonalized by a real-space Bogoliubov transformation [52] via

$$\begin{aligned} \eta_n &= \sum_j \left(u_{n,j} c_j + v_{n,j} c_j^\dagger \right), \\ \eta_n^\dagger &= \sum_j \left(u_{n,j} c_j^\dagger + v_{n,j} c_j \right). \end{aligned} \quad (21)$$

Here u_n and v_n are real coefficients. In order to have η_n as fermion operators, the following orthonormal relations are imposed:

$$\begin{aligned} \sum_j \left(u_{m,j} u_{n,j} + u_{m,j} v_{n,j} \right) &= \delta_{mn}, \\ \sum_j \left(u_{m,j} v_{n,j} + v_{m,j} u_{n,j} \right) &= 0. \end{aligned} \quad (22)$$

The Hamiltonian after the diagonalization becomes

$$H = \sum_n E_n \eta_n^\dagger \eta_n. \quad (23)$$

The anti-commutation relations between η_n then lead to

$$[\eta_m, H] = E_m \eta_m. \quad (24)$$

Substituting Eq. (20) and Eq. (21) into Eq. (24), we arrived at the BdG equations

$$\sum_j \left(T_{ij} u_{n,j} + V_{ij} v_{n,j} \right) = E_n u_{n,j}, \quad (25)$$

$$\sum_j \left(V_{ji} u_{n,j} - T_{ij} v_{n,j} \right) = E_n v_{n,j}. \quad (26)$$

The BdG equation has a particle-hole symmetry that pairs each $E_n > 0$ state with a $E_n < 0$ state, which allows us to further simplify the expressions.

Making use of the inverse Bogoliubov transformation

$$c_j = \sum_n \left(u_{n,j} \eta_n + v_{n,j} \eta_n^\dagger \right), \quad c_j^\dagger = \sum_n \left(u_{n,j} \eta_n^\dagger + v_{n,j} \eta_n \right), \quad (27)$$

we find that the pairing gap is determined by $\Delta_i = \sum_n [g_i u_{n,i} v_{n,i+1} [1 - f(E_n)] + g_i u_{n,i+1} v_{n,i} f(E_n)]$. Here $f(x) = 1/(e^{x/T} + 1)$ is the Fermi function. At $T = 0$, the gap function at site i is given by

$$\Delta_i = \sum_n \left[g_i u_{n,i} v_{n,i+1} \Theta(E_n) + g_i u_{n,i+1} v_{n,i} \Theta(-E_n) \right], \quad (28)$$

where $\Theta(x)$ is the step function. We remark that for the p -wave pairing of the Kitaev chain, the coefficients u_n, v_n may be chosen real [52] to simplify the expressions.

The BdG equation is solved by iterations. A trial form of Δ_i and a given μ are plugged into Eq. (25). After the diagonalization, the eigenvalues and eigenfunctions are found. A new gap function is then assembled according to Eq. (28). A new iteration begins until the convergence condition $(1/L) \sum_i |\Delta_i^{new} - \Delta_i^{old}| < \epsilon$. Here Δ_i^{new} and Δ_i^{old} are the profiles of the gap function between two adjacent iterations and L is the lattice size. We use $\epsilon = 10^{-4}$ in our calculation. After the iteration converges, the ground-state density at site i can be obtain by

$$n_i = \langle c_i^\dagger c_i \rangle = \sum_n \left[u_{n,i}^2 \Theta(E_n) + v_{n,i}^2 \Theta(-E_n) \right]. \quad (29)$$

III. QUENCH OF INTERACTION IN SPACE

When the pairing coupling constant g vanishes, the ground state of the Kitaev chain changes from a superfluid to a spin-polarized normal Fermi gas. With spatially inhomogeneous interactions, a quantum transition in real space may emerge as g drops to zero. There are many possible inhomogeneous profiles of the interactions. Here we follow Ref. [12] and investigate two types of quenches in real space illustrated in Fig. 1. The spatial quench has a linear ramp of the interaction while the step-function quench has an abrupt drop.

Since the gap function shown in Eq. (28) vanishes when $g_i = 0$, it does not reflect the penetration of the pairing into the normal-gas phase. Instead, we analyze the pair wavefunction $F_j = \langle c_j c_{j+1} \rangle$, which decays into the normal-gas phase and exhibits interesting scaling behavior.

A. Spatial quench

We consider a linear ramp of the pairing interaction, which allows for an analysis of the scaling behavior according to the spatial KZM. The coupling constant g linearly drops to zero inside the interval $\frac{L}{2} - L_1 < i < \frac{L}{2}$ with the profile

$$g_i = \begin{cases} g_0, & 1 \leq i \leq L/2 - L_1, \\ g_0 \frac{L/2 - i}{L_1}, & L/2 - L_1 \leq i \leq L/2, \\ 0, & L/2 < i \leq L. \end{cases} \quad (30)$$

As a consequence, a real-space QCP at $x_c = L/2$ emerges as g_i drops to zero, separating the superfluid phase on the left and the normal phase on the right. The ramp of the interaction profile introduces a slope $\alpha = g_0/(L_1)$, which plays the role of the quench rate of the time-dependent KZM [10].

Near the QCP at $x_c = L/2$, we may write $g_0 - \alpha(x - x_c) = -\alpha y$, where $y = (x - x_c - g_0/\alpha)$. In the ramp, the coherence length freezes at $\xi = \xi_{fr}$ due to the drop of the interaction. From Eq. (11) in the weakly interacting regime, the frozen coherence length leads to $\Delta_{fr} \sim \exp(-1/g_{fr}) \sim \exp(1/(\alpha \xi_{fr}))$. Since the ramp occurs in the superfluid regime, the BCS coherence length given by Eq. (15) leads to a consistent equation for ξ_{fr} , given by $\xi_{fr} \sim (1/\Delta_{fr}) \sim \exp(-1/(\alpha \xi_{fr}))$. The frozen coherence length determines the correlation on the other side of the QCP, so the characteristic length ξ_F of the pair wavefunction on the normal-gas region is determined by ξ_{fr} . Therefore, we obtain the scaling

$$\xi_F \ln(\xi_F) \sim 1/\alpha. \quad (31)$$

This is different from the power-law scaling behavior of the spatial KZM in magnetic systems [7, 8] because the order parameter of the BCS theory, which is the gap function, is nonanalytic in the interaction strength even in the weakly interacting regime. The correlation length is thus dominated by the nonanalytic behavior and exhibits interesting scaling behavior as the system crosses a superfluid to normal-gas QCP in real space. We mention if the correlation length diverges near the critical point according to a power law $\xi \sim \epsilon^{-\nu}$ like the TFIM, where ϵ measures the distance to the transition, the freezing length ξ_{fr} occurs when $\epsilon_{fr} \sim \alpha \xi_{fr}$, where α is the slope of the spatial quench. Therefore, $\xi \sim \alpha^{-\nu/(1+\nu)}$ for the conventional characteristic length from the spatial KZM.

B. Step-function quench

The step-function quench with a sudden drop of the coupling constant g in the middle of the chain may be considered as a limiting case of the spatial quench when the ramp is infinitely narrow. Explicitly, the location-dependent coupling constant follows the equation

$$g_i = \begin{cases} g_0, & 1 \leq i \leq L/2, \\ 0, & L/2 < i \leq L. \end{cases} \quad (32)$$

When g_i drops to zero, the system transitions from a superfluid to a normal gas. Therefore, a QCP in real space is present at $x_c = L/2$. The sudden drop of the pairing interaction leaves no additional length scale other than the BCS coherence length for the fermion pairs. Therefore, the characteristic length ξ_F of the penetration of the pair wavefunction F in the normal region is expected to follow the scaling relation

$$\ln(\xi_F) \sim g_0^{-1} \quad (33)$$

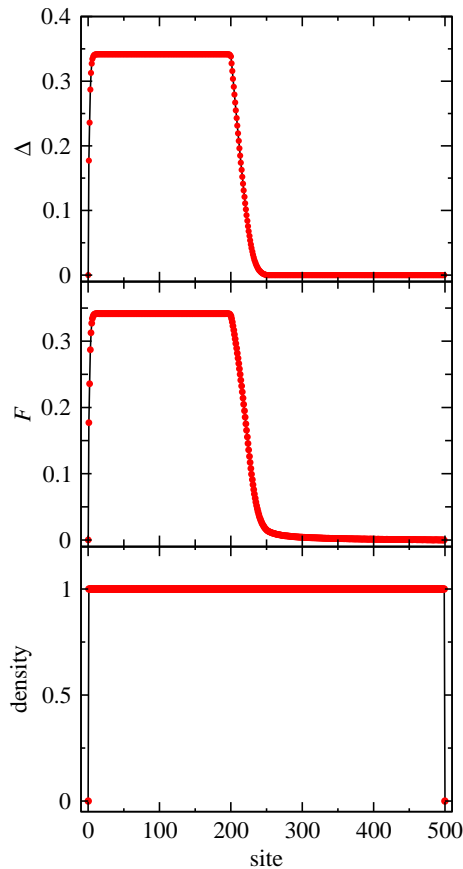


Figure 2. Profiles of the gap function (top panel), pair wavefunction $F_i = \langle c_i c_{i+1} \rangle$ (middle panel), and density (bottom panel) as functions of the site index of a spatial quench. Here $g_0 = 1$, $\mu = 0$, $L = 500$, and the ramp width is $L_1 = 50$.

in the weak interaction regime similar to that of the BCS coherence length of Eq. (15) in the bulk of the superfluid region.

IV. RESULTS AND DISCUSSIONS

A. Scaling analyses

Here we show our solutions of the BdG equation with open boundary condition. Up to 1000 sites in the system have been analyzed to obtain the scaling behavior of the pair wavefunction in the normal-gas region. We first show the profiles of the gap function, F_j , and density as functions of the site index for a selected case undergoing a spatial quench in Fig. 2. Due to the vanishing g_i at $x_c = L/2$, the gap function drops to zero at x_c as well. However, the pair wavefunction continuously extends into the normal-gas region. On the other hand, the density is basically flat across the QCP in real space, as pairing in the BCS regime does not introduce drastic changes to the expression of the density. The introduction of a linear ramp in the interaction profile results in

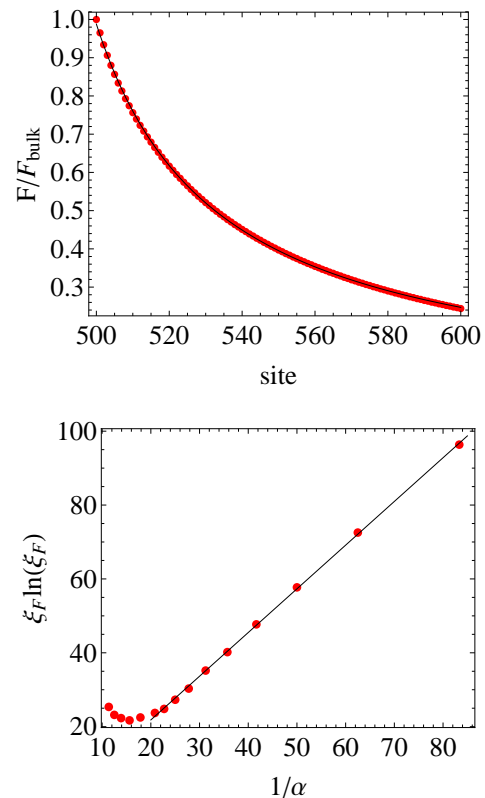


Figure 3. (Top) Fitting of the pair wavefunction F by Eq. (34) in the normal-gas region in a spatial quench. Here $g_0 = 1$, $\mu = 0$, $L = 1000$, and the ramp width is $L_1 = 100$. (Bottom) The characteristic length ξ_F extracted from the fitting of F in the normal-gas region as a function of $1/\alpha$ (red dots). The black line is Eq. (31). A deviation from the weak-interaction prediction is visible when $1/\alpha$ decreases.

interesting scaling behavior, which we will analyze here.

To fit the decay of the pair wavefunction F in the normal-gas region, we refine the grid and zoom in the right-half of the solutions. For s -wave pairing in continuum, it has been shown [53–55] that the decay of F in the normal-gas region at zero temperature follows the power-law form

$$F(x) \sim \frac{\xi_F}{x - x_c}. \quad (34)$$

Although here we study p -wave pairing in a lattice system, we found the power-law form still fits our data well, as shown in the left panel of Fig. 3. The fitting allows us to extract the characteristic length ξ_F for a particular set of parameters. After collecting more values of ξ_F as a function of the ramp slope $\alpha = g_0/L_1$ of the pairing interactions, we compare the data with the functional form of Eq. (31) from the spatial KZM in the weak-interaction regime, as shown in the right panel of Fig. 3. The agreement between the numerical simulations and analytic formula in the weak-interaction regime shows the universal behavior of the spatial KZM applied to p -wave

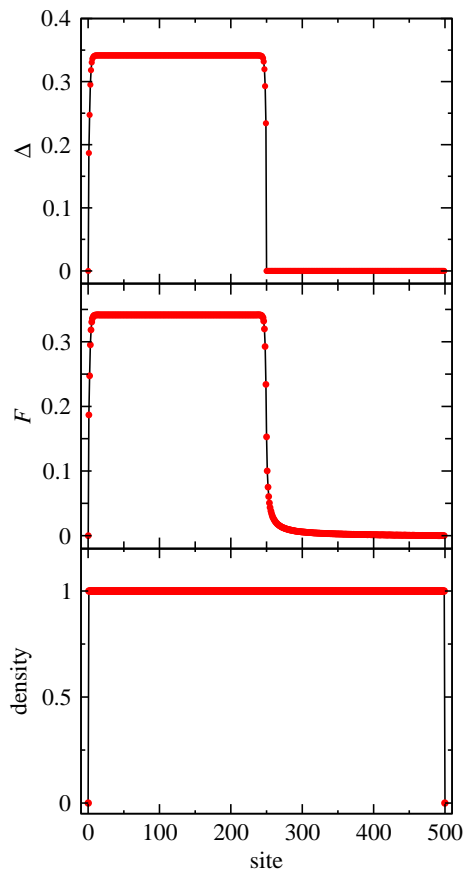


Figure 4. Profiles of the gap function (top panel), pair wavefunction $F_i = \langle c_i c_{i+1} \rangle$ (middle panel), and density (bottom panel) as functions of the site index for a step-function quench of Eq. (32). Here we assume $g_0 = 1$, $\mu = 0$ and the system size is $L = 500$.

Fermi superfluids described by the mean-field BCS theory in the ground state. Away from the weak-interaction regime when $1/\alpha$ becomes small, however, the characteristic length ξ_F starts to deviate from the weak-interaction prediction because the analytic expression (31) no longer applies although the fitting of F by Eq (34) still works.

On the other hand, the profiles of the gap function Δ , pair wavefunction $F_j = \langle c_j c_{j+1} \rangle$, and density as functions of the site index following a step-function quench are shown in Fig. 4. At first look, they are very similar to their counterparts in the spatial quench. However, the vanishing of the width of the ramp leads to a different scaling analysis for the step-function quench because there is no longer an additional length scale (from the slope) as the system crosses the QCP in real space.

The fitting of F in the normal-gas region of a selected step-function quench case with the form of Eq. (34) is shown in the left panel of Fig. 5, which allows us to extract the value of the characteristic length ξ_F for this set of parameters. By extracting ξ_F as a function of g_0 , we show the scaling behavior of ξ_F in the right panel of Fig 5. One can see that the scaling agrees with Eq. (33) in the

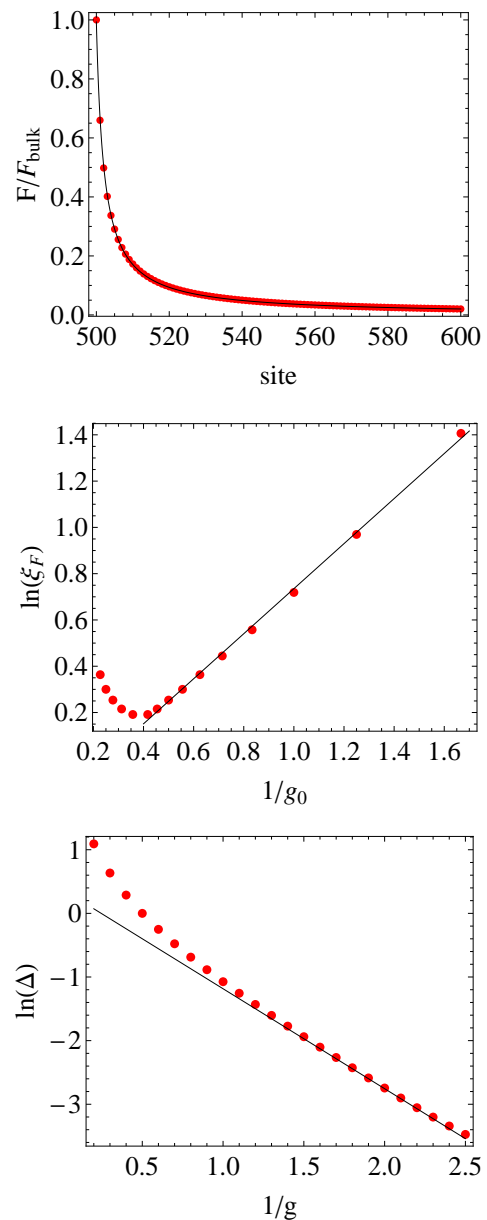


Figure 5. (Top) Fitting of the pair wavefunction F in the normal-gas region by Eq. (34). Here $g_0 = 1$, $\mu = 0$ with $L = 1000$. (Middle) $\ln \xi_F$ as a function of $1/g_0$ (red dots) and the BCS coherence length of the superfluid region in the weak-interaction regime (black line). (Bottom) Δ as a function of $1/g$ for a uniform Kitaev chain with $\mu = 0$ (red dots). The black line shows Eq. (11) from the weak-interaction regime. Deviations from the weak-interaction predictions are observable in the middle and bottom panels.

weak-interaction regime. Therefore, the BCS coherence length on the superfluid side determines the penetration of the pair wavefunction into the normal-gas region because there is no additional length scale in a step-function quench across the QCP in real space. As g_0 increases, ξ_F shows a deviation from the weak-interaction prediction. The reason is because the BCS gap function deviates

from the weak-interaction expression (11) as g_0 increases since we have verified the fitting of F by Eq. (34) still works well when g_0 is large. To visualize the deviation of Δ from the weak-interaction expression, we show in the bottom panel of Fig 5 the gap function of a homogeneous Kitaev chain compared to the weak-interaction formula (11).

We have two remarks about the results: (1) Our solutions to the BdG equation only cover a limited range of the interaction or its slope. If g_0 is too small or α is too large, the bulk gap becomes exponentially small due to Eq. (11). It is difficult for the numerical iterations to converge. The small value of the pair wavefunction also makes it challenging to extract the correct value on the normal-gas side. On the other hand, if g_0 is too large or the slope is too steep, the convergence of the BdG equation becomes slow because a small adjustment may lead to a substantial change in the related quantities. Moreover, a strong pairing interaction on the left side pushes the system away from the BCS regime, making it challenging to have a continuous connection with the normal-gas region on the right. Nevertheless, we managed to obtain enough results to demonstrate the agreements of the scaling behavior in the weak-interaction regime and the deviations from the weak-interaction predictions away from that regime. (2) We have checked other values of μ and found that while there are quantitative changes in the density profile, the scaling behavior of both spatial quench and step-function quench remain the same as the $\mu = 0$ case for a reasonable range of the interaction profiles. An illustration of the profiles of Δ , F , and density for the case with $\mu = 0.5$ in a step-function quench is shown in Fig. 6. While there are wiggles in the density profile, the pair wavefunction remains smooth and its penetration in the normal-gas region follows the same scaling as that of the $\mu = 0$ case, so we will not repeat the results here.

B. Energy spectrum and eigenstates

Here we investigate the states of the Kitaev chain in the presence of a hard-wall box potential and spatially varying pairing interactions. The BdG equation allows us to analyze both the energy spectrum and the profiles of individual states. Fig. 7 shows the eigen-energies and some selected states for a a step-function quench. To contrast the features from the inhomogeneous interaction profile with the homogeneous one, we plot in the same panel the energy spectrum of a similar system with a homogeneous interaction profile of g_0 . While the bulk bands are alike, one can see that there are many in-gap states for the step-function quench case. We will show that there are two types of in-gap states, one from the localization at the hard wall on the superfluid side and the other from the unpaired fermions on the right half of the chain.

For the step-function case, some selected wave func-

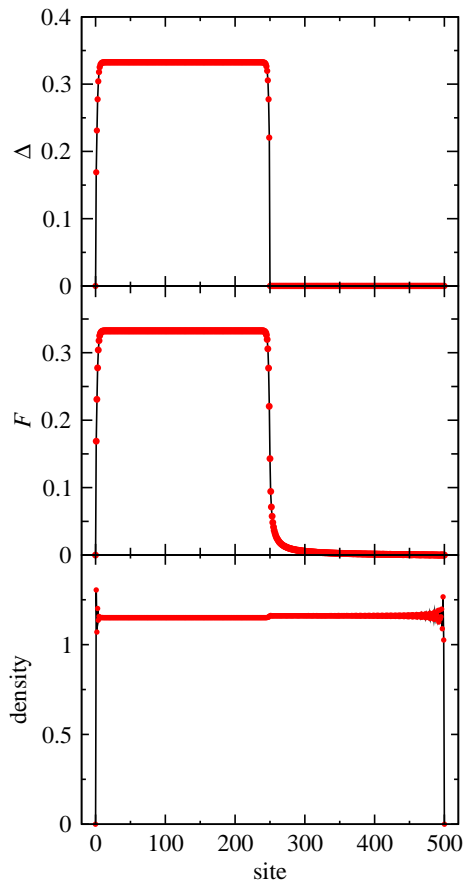


Figure 6. Profiles of Δ (top), F (middle), and density (bottom) for a step-function quench with $\mu = 0.5$. Here $g_0 = 1$ and $L = 500$.

tions u_n in the bulk band, near zero energy, and inside the energy gap as functions of the site index from the BdG equation are shown in Fig. 7. The top-right panel is a bulk state with its amplitude spreading over the whole chain. The lower-left panel shows the state near $E = 0$, which localizes at the left hard wall. The hard wall may be viewed as a boundary between the fermions and vacuum, so a localized edge state can be trapped there in the topological regime. This type of in-gap states is also present when the profile of g_0 is uniform. According to Eq. (18), the system is indeed topological when $\mu = 0$ for the half-filling case. Finally, the bottom-right panel shows a state inside the energy gap but away from $E = 0$. It displays non-zero amplitude only in the region where $g_i = 0$, thereby representing a normal-gas state due to the vanishing pairing interaction on the right half.

C. Implications

While the spatial KZM of TFIM has been shown to exhibit power-law scaling of the decaying order parameter in the symmetric phase [7, 8], the non-analytic behavior of the BCS theory leads to complicated scaling behav-

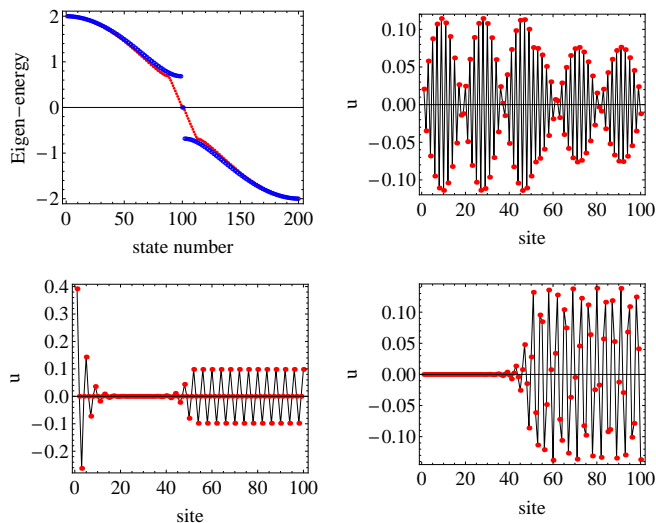


Figure 7. (Top left) Energy spectra of a step-function quenched system (small red dots) and a homogeneous system (large blue circles). For the step-function quench, the wavefunction u of a typical bulk state in the upper band, an edge state near zero energy, and a normal-gas state with $E \approx 0.3$ are shown in the top-right, bottom-left, and bottom-right panels, respectively. Here v behaves similarly as u , and $L = 100$ for better visualization of the wavefunctions.

ior, as pointed out in Ref. [12] and here. Our results thus demonstrate the variety and versatility of the spatial KZM as a general framework. While the freezing of the coherence length due to the linear ramp applies to general types of phase transitions, the scaling behavior depends on the functional forms from the underlying systems. The peculiar scaling of the BCS theory across a QPT in real space thus provides another exotic feature of fermionic superfluids. We remark that if a bosonic system is considered instead, turning off the interaction between bosons leaves a Bose-Einstein condensate of non-interacting bosons at $T = 0$, which is still considered as a symmetry-broken phase and makes it different from the fermionic case studied here.

There are several differences between the p -wave superfluid and the s -wave one studied in Ref. [12]: (1) The p -wave pairing is between single-component (spin-polarized) fermions while the s -wave pairing is between two-component fermions. (2) The p -wave pairing is between adjacent lattice sites while the s -wave pairing is on-site. As a consequence, the pair wavefunction F is on-site for s -wave pairing but between adjacent sites for p -wave pairing. (3) The Kitaev chain describes a topological superfluid with properties absent in the s -wave model.

Nevertheless, we have shown that the functional forms of the order parameter represented by the gap function and the BCS coherence length are similar for the s -wave and p -wave pairing cases in the weak-interaction regime. Thus, their scaling behavior will be similar at least in that regime. While Ref. [12] did not explore the deviations from the weak-interaction regime due to numerical complications, here we have demonstrated the deviations of the Kitaev chain because of the simplifications summarized above for the p -wave Fermi superfluids in spatial and step-function quenches.

There have been many attempts to realize the Kitaev chain, including those using quantum dots [56] and theoretical work cautioning some subtleties [57] (see also Ref. [58] for a review). Moreover, quantum simulators or computers also offer insights into the Kitaev chain [59–63]. Since the attractive interactions are induced or effective in most settings, it may be possible to tune the attraction in real space by varying the chemical or physical properties, such as the composition, electric or magnetic field, strain, light-matter interactions or other means, of the systems or simulators of the Kitaev chain to generate the inhomogeneous interactions studied in this work.

V. CONCLUSION

The BdG equation of a p -wave Fermi superfluid described by the Kitaev chain with inhomogeneous pairing interaction profiles has revealed how the remnant of the pair wavefunction survives in the normal-gas region as the system in equilibrium exhibits a quantum critical point in real space. The mean-field BCS analysis leads to scaling behavior of the spatial and step-function quenches confirmed by the BdG equation in the weak- and intermediate- interaction regimes. The linear ramp of the spatial quench introduces an additional length scale from the slope, resulting in the spatial KZM, while the step-function quench is dominated by the BCS coherence length on the superfluid side. The energy spectrum and eigenfunctions further distinguish the topological edge states from the normal-gas states. Our study thus offers another example of using inhomogeneity to explore complex quantum systems.

ACKNOWLEDGMENTS

Y. H. was supported by the NNSF of China (No. 11874272) and Science Specialty Program of Sichuan University (No. 2020SCUNL210). C. C. C. was partly supported by the NSF (No. PHY-2310656).

[1] S. L. Sondhi, S. M. Girvin, J. P. Carini, and D. Shahar, Rev. Mod. Phys. **69**, 315 (1997), URL

<https://link.aps.org/doi/10.1103/RevModPhys.69.315>.

- [2] M. Vojta, Rep. Prog. Phys. **66**, 2069 (2003), URL <https://dx.doi.org/10.1088/0034-4885/66/12/R01>.
- [3] S. Sachdev, *Quantum Phase Transitions* (Cambridge University Press, Cambridge, UK, 2011), 2nd ed.
- [4] L. D. Carr, ed., *Understanding Quantum Phase Transitions* (CRC Press, Boca Raton, 2010).
- [5] A. Dutta, G. Aeppli, B. K. Chakrabarti, U. Divakaran, T. F. Rosenbaum, and D. Sen, *Quantum Phase Transitions in Transverse Field Spin Models: From Statistical Physics to Quantum Information* (Cambridge University Press, Cambridge, UK, 2015).
- [6] A. J. Leggett, *Quantum Liquids : Bose condensation and Cooper pairing in condensed-matter systems*, Oxford Graduate Texts (Oxford University Press, Oxford, UK, 2006), ISBN 0198526431.
- [7] W. H. Zurek and U. Dorner, Philos. Trans. Royal Soc. A **366**, 2953 (2008), ISSN 1364-503X.
- [8] J. Dziarmaga and M. M. Rams, New J. Phys. **12**, 055007 (2010), ISSN 1367-2630.
- [9] B. Damski and W. H. Zurek, New J. Phys. **11**, 063014 (2009), URL <https://dx.doi.org/10.1088/1367-2630/11/6/063014>.
- [10] J. Dziarmaga, Adv. Phys. **59**, 1063 (2010), ISSN 0001-8732.
- [11] M. Lacki and B. Damski, J. Stat. Mech. p. 103105 (2017).
- [12] B. Parajuli and C.-C. Chien, Phys. Rev. A **107**, 063314 (2023), URL <https://link.aps.org/doi/10.1103/PhysRevA.107.063314>
- [13] A. Y. Kitaev, Phys. Usp. **44**, 131 (2001).
- [14] P. G. De Gennes, *Superconductivity of Metals and Alloys.*, Advanced Books Classics (Chapman and Hall/CRC, Boulder, 2018), 2nd ed., ISBN 9780429965586.
- [15] J.-X. Zhu, *Bogoliubov-de Gennes Method and Its Applications*, Lecture Notes in Physics, 924 (Springer International Publishing, Cham, 2016), 1st ed., ISBN 3-319-31314-2.
- [16] M. Z. Hasan and C. L. Kane, Rev. Mod. Phys. **82**, 3045 (2010).
- [17] X.-L. Qi and S.-C. Zhang, Rev. Mod. Phys. **83**, 1057 (2011).
- [18] C. K. Chiu, J. C. Y. Teo, A. P. Schnyder, and S. Ryu, Rev. Mod. Phys. **88**, 035005 (2016).
- [19] L. Fu and C. L. Kane, Phys. Rev. Lett. **100**, 096407 (2008), URL <https://link.aps.org/doi/10.1103/PhysRevLett.100.096407>.
- [20] T. W. B. Kibble, J. Phys. A: Math. Gen. **9**, 1387 (1976), URL <https://dx.doi.org/10.1088/0305-4470/9/8/029>.
- [21] T. Kibble, Phys. Rep. **67**, 183 (1980), ISSN 0370-1573, URL <https://www.sciencedirect.com/science/article/pii/037015738090015>
- [22] W. H. Zurek, Nature (London) **317**, 505 (1985), ISSN 0028-0836.
- [23] W. Zurek, Phys. Rep. **276**, 177 (1996), URL <https://doi.org/10.1016/2Fs0370-1573%2896%2900009-9>.
- [24] P. Laguna and W. H. Zurek, Phys. Rev. Lett. **78**, 2519 (1997), URL <https://link.aps.org/doi/10.1103/PhysRevLett.78.2519>.
- [25] J. R. Anglin and W. H. Zurek, Phys. Rev. Lett. **83**, 1707 (1999), URL <https://link.aps.org/doi/10.1103/PhysRevLett.83.1707>.
- [26] G. J. Stephens, L. M. A. Bettencourt, and W. H. Zurek, Phys. Rev. Lett. **88**, 137004 (2002), URL <https://link.aps.org/doi/10.1103/PhysRevLett.88.137004>.
- [27] J. Dziarmaga, Phys. Rev. Lett. **95**, 245701 (2005), URL <https://link.aps.org/doi/10.1103/PhysRevLett.95.245701>.
- [28] W. H. Zurek, U. Dorner, and P. Zoller, Phys. Rev. Lett. **95**, 105701 (2005), URL <https://link.aps.org/doi/10.1103/PhysRevLett.95.105701>.
- [29] D. Jaschke, K. Maeda, J. D. Whalen, M. L. Wall, and L. D. Carr, New J. Phys. **19**, 033032 (2017), URL <https://dx.doi.org/10.1088/1367-2630/aa65bc>.
- [30] J. Dziarmaga, M. M. Rams, and W. H. Zurek, Phys. Rev. Lett. **129**, 260407 (2022), URL <https://doi.org/10.1103/physrevlett.129.260407>.
- [31] M. Uhlmann, R. Schützhold, and U. R. Fischer, Phys. Rev. D **81**, 025017 (2010), URL <https://link.aps.org/doi/10.1103/PhysRevD.81.025017>.
- [32] M. Uhlmann, R. Schützhold, and U. R. Fischer, New J. Phys. **12**, 095020 (2010), URL <https://dx.doi.org/10.1088/1367-2630/12/9/095020>.
- [33] A. Polkovnikov, Phys. Rev. B **72**, 161201(R) (2005), URL <https://link.aps.org/doi/10.1103/PhysRevB.72.161201>.
- [34] G. L. Warner and A. J. Leggett, Phys. Rev. B **71**, 134514 (2005), URL <https://link.aps.org/doi/10.1103/PhysRevB.71.134514>.
- [35] K. Shimizu, Y. Kuno, T. Hirano, and I. Ichinose, Phys. Rev. A **97**, 033626 (2018), URL <https://link.aps.org/doi/10.1103/PhysRevA.97.033626>.
- [36] F. M. Cucchiatti, B. Damski, J. Dziarmaga, and W. H. Zurek, Phys. Rev. A **75**, 023603 (2007), URL <https://link.aps.org/doi/10.1103/PhysRevA.75.023603>.
- [37] J. Dziarmaga, M. Tylutki, and W. H. Zurek, Phys. Rev. B **86**, 144521 (2012), URL <https://link.aps.org/doi/10.1103/PhysRevB.86.144521>.
- [38] B. Gardas, J. Dziarmaga, and W. H. Zurek, Phys. Rev. B **95**, 104306 (2017), URL <https://link.aps.org/doi/10.1103/PhysRevB.95.104306>.
- [39] Y. Machida and K. Kasamatsu, Phys. Rev. A **103**, 013310 (2021), URL <https://link.aps.org/doi/10.1103/PhysRevA.103.013310>.
- [40] R. Monaco, J. Mygind, and R. J. Rivers, Phys. Rev. Lett. **89**, 080603 (2002), URL <https://link.aps.org/doi/10.1103/PhysRevLett.89.080603>.
- [41] S. Ulm, J. Rosnagel, G. Jacob, C. Deguenther, S. T. Dawkins, U. G. Poschinger, R. Nigmatullin, A. Retzker, M. B. Plenio, F. Schmidt-Kaler, et al., Nat. Commun. **4**, 2290 (2013), ISSN 2041-1723.
- [42] K. Pyka, J. Keller, H. L. Partner, R. Nigmatullin, T. Burgermeister, D. M. Meier, K. Kuhlmann, A. Retzker, M. B. Plenio, W. H. Zurek, et al., Nat. Commun. **4**, 2291 (2013), ISSN 2041-1723.
- [43] N. Navon, A. L. Gaunt, R. P. Smith, and D. Barak, Science **347**, 167 (2015), <https://www.science.org/doi/pdf/10.1126/science.1258676>, URL <https://www.science.org/doi/abs/10.1126/science.1258676>
- [44] S. Braun, M. Friesdorf, S. S. Hodgman, M. Schreiber, J. P. Ronzheimer, A. Riera, M. del Rey, I. Bloch, J. Eisert, and U. Schneider, PNAS **112**, 3641 (2015), <https://www.pnas.org/doi/pdf/10.1073/pnas.1408861112>, URL <https://www.pnas.org/doi/abs/10.1073/pnas.1408861112>.
- [45] D. Chen, M. White, C. Borries, and B. DeMarco, Phys. Rev. Lett. **106**, 235304 (2011), URL <https://link.aps.org/doi/10.1103/PhysRevLett.106.235304>.
- [46] A. Keesling, A. Omran, H. Levine, H. Bernien, H. Pichler, S. Choi, R. Samajdar, S. Schwartz, P. Silvi,

- S. Sachdev, et al., *Nature* **568**, 207 (2019), ISSN 0028-0836.
- [47] M. Anquez, B. A. Robbins, H. M. Bharath, M. Boguslawski, T. M. Hoang, and M. S. Chapman, *Phys. Rev. Lett.* **116**, 155301 (2016), URL <https://link.aps.org/doi/10.1103/PhysRevLett.116.155301>.
- [48] B.-W. Li, Y.-K. Wu, Q.-X. Mei, R. Yao, W.-Q. Lian, M.-L. Cai, Y. Wang, B.-X. Qi, L. Yao, L. He, et al., *PRX Quantum* **4**, 010302 (2023), URL <https://link.aps.org/doi/10.1103/PRXQuantum.4.010302>.
- [49] S. Deuschländer, P. Dillmann, G. Maret, and P. Keim, *PNAS* **112**, 6925 (2015), <https://www.pnas.org/doi/pdf/10.1073/pnas.1500763112>, URL <https://www.pnas.org/doi/abs/10.1073/pnas.1500763112>.
- [50] B. Ko, J. W. Park, and Y. Shin, *Nat. Phys.* **15**, 1227 (2019), ISSN 1745-2473.
- [51] X.-P. Liu, X.-C. Yao, Y. Deng, Y.-X. Wang, X.-Q. Wang, X. Li, Q. Chen, Y.-A. Chen, and J.-W. Pan, *Phys. Rev. Res.* **3**, 043115 (2021), URL <https://link.aps.org/doi/10.1103/PhysRevResearch.3.043115>.
- [52] E. Lieb, T. Schultz, and D. Mattis, *Annals of Physics* **16**, 407 (1961), ISSN 0003-4916, URL <https://www.sciencedirect.com/science/article/pii/00034916619001154>.
- [53] G. Deutscher and P. de Gennes, pp 1005-34 of *Superconductivity*. Vols. 1 and 2. Parks, R. D. (ed.). New York, Marcel Dekker, Inc., 1969 (1969).
- [54] D. S. Falk, *Phys. Rev.* **132**, 1576 (1963), URL <https://link.aps.org/doi/10.1103/PhysRev.132.1576>.
- [55] W. Silvert, *Rev. Mod. Phys.* **36**, 251 (1964), URL <https://link.aps.org/doi/10.1103/RevModPhys.36.251>.
- [56] T. Dvir, G. Wang, N. van Loo, C.-X. Liu, G. P. Mazur, A. Bordin, S. L. D. ten Haaf, J.-Y. Wang, D. van Driel, F. Zatelli, et al., *Nature* **614**, 445 (2023), ISSN 1476-4687, URL <https://doi.org/10.1038/s41586-022-05585-1>.
- [57] H. Pan and S. Das Sarma, *Phys. Rev. B* **107**, 035440 (2023), URL <https://link.aps.org/doi/10.1103/PhysRevB.107.035440>.
- [58] F. v. Oppen, Y. Peng, and F. Pientka, in *Topological Aspects of Condensed Matter Physics: Lecture Notes of the Les Houches Summer School: Volume 103, August 2014* (Oxford University Press, 2017), ISBN 9780198785781, <https://academic.oup.com/book/0/chapter/203983732/chapter-pdf/45122673/acprof-9780198785781-chapter-9.pdf>, URL <https://doi.org/10.1093/acprof:oso/9780198785781.003.0003>.
- [59] J. P. T. Stenger, N. T. Bronn, D. J. Egger, and D. Pekker, *Phys. Rev. Research* **3**, 033171 (2021).
- [60] H.-L. Huang, M. Naroźniak, F. Liang, Y. Zhao, A. D. Castellano, M. Gong, Y. Wu, S. Wang, J. Lin, Y. Xu, et al., *Phys. Rev. Lett.* **126**, 090502 (2021), URL <https://link.aps.org/doi/10.1103/PhysRevLett.126.090502>.
- [61] X. Mi, M. Sonner, M. Y. Niu, K. W. Lee, B. Foxen, I. Aleiner, T. I. Andersen, F. Arute, K. Arya, et al., *Science* **378**, 785 (2022).
- [62] M. J. Rančić, *Sci. Rep.* **12**, 19882 (2022), ISSN 2045-2322, URL <https://doi.org/10.1038/s41598-022-24341-z>.
- [63] T. Iizuka, H. Yuan, Y. Mita, A. Higo, S. Yasunaga, and M. Ezawa, *Commun. Phys.* **6**, 279 (2023), ISSN 2399-3650, URL <https://doi.org/10.1038/s42005-023-01404-9>.